GROUND TRUTH HYPOCENTERS AND 3D CRUSTAL VELOCITY STRUCTURE IN CENTRAL ASIA FROM IN-COUNTRY NETWORKS

Thomas de la Torre[1], Gaspar Monsalve-Mejia[1], Anne F. Sheehan[1], Charlotte Rowe[2], and Michael Begnaud[2]

University of Colorado at Boulder[1] and Los Alamos National Laboratory[2]

Sponsored by National Nuclear Security Administration
Office of Nonproliferation Research and Development
Office of Defense Nuclear Nonproliferation

Contract Nos. DE-FC52-04NA25544[1] and W-7405-ENG-36[2]

ABSTRACT

The Himalayan Nepal Tibet Seismic Experiment (HIMNT) consisted of 28 broadband STS2 seismometers deployed throughout eastern Nepal and the southern Tibetan Plateau during 2001–2003. The data set is unique, with many stations in remote and difficult to access locations. Ground truth coverage in this portion of Asia is sparse and no permanent stations exist in most of the area covered by the HIMNT network. Thus this unique data set is able to provide reference events where none previously existed. With the ray coverage afforded us by the HIMNT and other regional stations and local network data, we are able to improve the regional and local velocity model as well, through 3D tomographic inversion.

We have examined the entire continuous HIMNT seismic data set and have picked and located over 1600 regional and local events, ranging in magnitude from 1 to 5.5. Initial hypocenters are determined using a priori 1D velocity models and a weighted least squares location algorithm. Relocations using the 1D velocity models result in 33 events that pass the ground truth (GT) criteria of Bondar et al. (2004) for GT5. We further refine the earthquake hypocenters by inverting for 2D and 3D velocity structure with earthquake relocation using the code SIMUL2000. These 2D and 3D locations should increase the number of ground truth events available. Teleseismic receiver function analysis is used to further constrain the crustal thickness variations and the geometry of the major interfaces. The Vp/Vs structure obtained from local earthquake tomography shows a noticeable contrast between the Indian Plate and the overlying thrust sheet, at the bottom of which we find a region of high S-wave speed. Upper mantle P-wave speeds in the study are unusually high, but do not appear to be related to anisotropy. Earthquake hypocenters delineate several distinct groupings that correlate with tectonics of the collision zone. Crustal earthquakes show alignments with depths less than 25 km along the region of highest relief of the Himalayan Front. Clusters of upper mantle earthquakes are found beneath the High Himalaya, in the southern Tibetan Plateau, and beneath southern Nepal. We observe earthquake hypocenters over a large range of depths, beneath Nepal from near-surface to 65 km depth, and beneath the Tibetan Plateau from near-surface to 90 km depth. Earthquakes show a bimodal distribution with depth, with the greatest concentration of seismic events in the upper crust and around Moho depth.

Development of our GT catalog includes moment tensor analysis and waveform modeling of GT events with particular attention to depth control. We have determined focal mechanisms from moment tensor inversion and first motion polarities for twelve of the largest and best recorded local earthquakes recorded during the HIMNT experiment and one ground truth event. We performed a grid search over source depth and different velocity model to examine the sensitivity of the fault plane solution and focal depth to crustal thickness and speed variations. The mostly strike-slip focal mechanisms at sub-Moho depths indicate a right lateral shear zone in the upper mantle beneath the Himalayas and the southern Tibetan Plateau. The new ground truth events can be used to calibrate station-centric correction surfaces and increase the ability to accurately locate and identify seismic events in these regions.

OBJECTIVES

The goal of this project is to contribute to the database of ground truth seismic events in central Asia using data from the Himalayan Nepal Tibet Seismic Experiment (HIMNT) network and other regional seismic data.

RESEARCH ACCOMPLISHED

HIMNT Deployment

The Himalayan Nepal Tibet Seismic Experiment (HIMNT) was a National Science Foundation (Program for Array Studies of the Continental Lithosphere PASSCAL) deployment in Nepal and Tibet in 2001–2003 (Figure 1). HIMNT was the first broadband seismic experiment to simultaneously cover the plains of southern Nepal, the Lesser and Greater Himalaya, and the Southern Tibetan Plateau. The HIMNT experiment included the deployment of twenty-eight three-component broadband seismic stations, which recorded continuously at a sample rate of 40–50 sps. Although the project has primarily tectonic objectives, the high-quality data collected are ideal for ground truth data for monitoring purposes. HIMNT stations were installed with approximately 40–50 km station spacing, covering a 2D area approximately 300 km wide east-west by 300 km north-south.

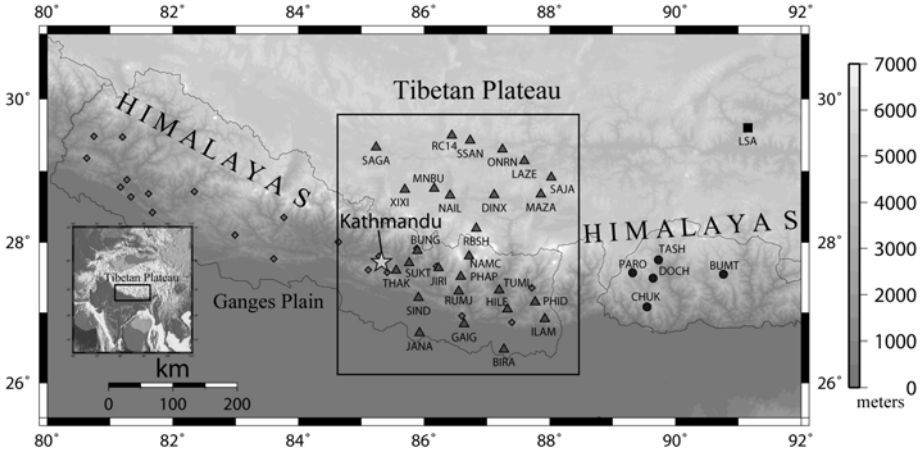

Figure 1. Topography of the study area and HIMNT broadband seismic 2001–2003 station network, triangles inside the rectangle. The moment tensor study was supplemented with data from the 2002 Bhutan broadband experiment (circles), the permanent Global Seismic Network station LSA (square), and the permanent National Seismological Network of Nepal (diamonds). A four letter code for each broadband station is shown.

Three-Dimensional Seismic Velocity Structure

We used P and S arrival time data from 542 earthquakes recorded by the network in order to simultaneously invert for earthquake location, and P-wave speed (Vp) and P- to S-wave speed ratio (Vp/Vs) for a 3D grid of nodes. A total of 5767 P-wave arrivals and 4801 S-wave arrivals were inverted using a method developed by Thurber (1983, 1993) and Eberhart-Phillips (1986), with the program SIMUL2000. The idea was to find the model that minimized the arrival time residuals at the stations. The technique consisted of an iterative damped least squares minimization algorithm. The travel times of the waves between source and receiver were determined by an approximate ray-tracing method (Thurber, 1983).

Several model parameterizations were tested, using an approach similar to that described by Husen et al. (2000), Eberhart-Phillips (1990), and Eberhart-Phillips and Michael (1998) in which we started solving for velocity structure at coarse grids of nodes, and progressively went to finer ones. The best model

parameterization was chosen based on arrival time misfit and the spread function of the resolution matrix. This function measured how similar the model resolution matrix is to the identity matrix (Menke, 1989; Toomey and Foulger, 1989; Michelini and McEvilly, 1991). The chosen model has a 50 km node spacing in the north-south and east-west directions and a vertical node separation of around 15 km. Depths went from surface to 70 km below sea level. After inversion, the obtained RMS arrival time residual was 0.31 s.

Figure 2 illustrates the values of P-wave speed at six different depths beneath the area of the network. Only areas with an associated diagonal resolution greater than 0.2 are shown. Similarly, Figure 3 shows Vp:Vs ratios for the same depths. This 3D velocity structure is then used in order to locate earthquakes in the study area, as discussed in the next section.

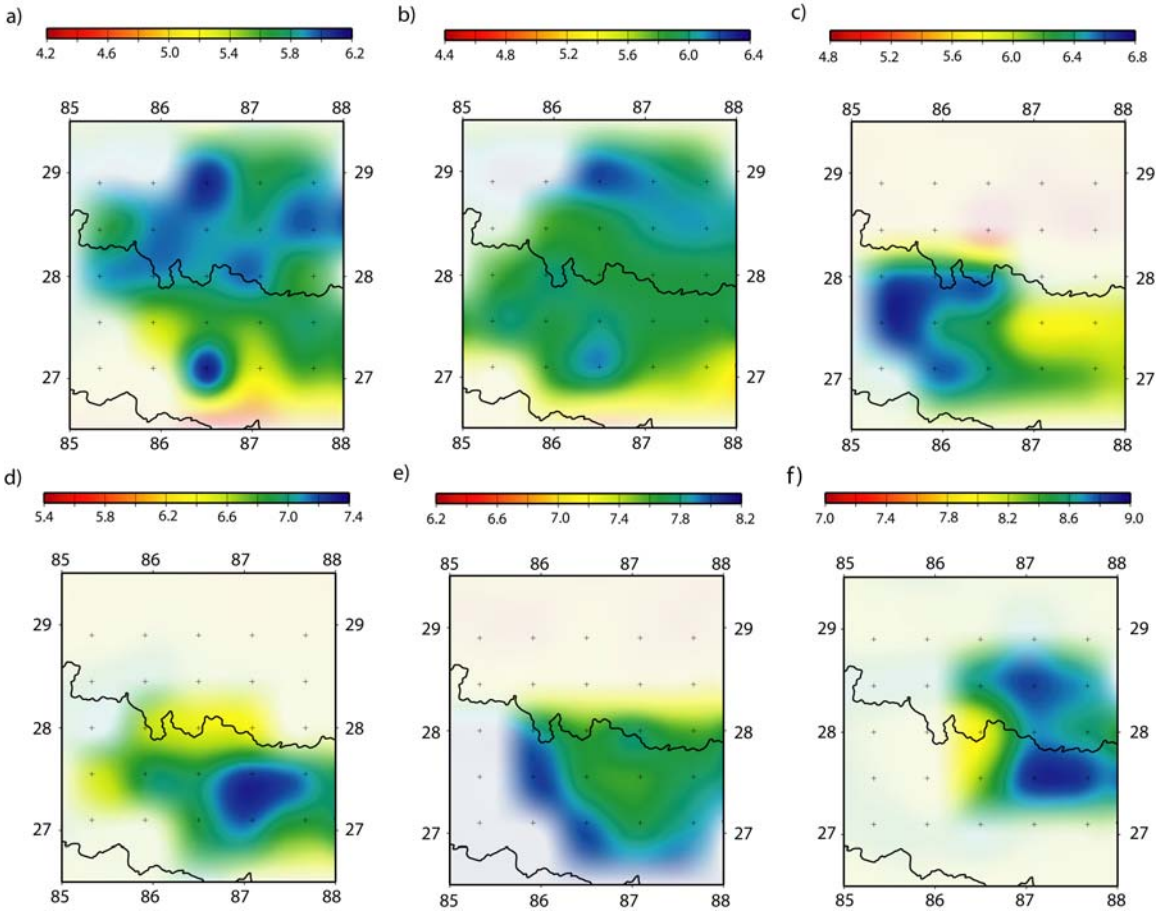

Figure 2. Three-dimensional velocity model used for earthquake locations. Horizontal sections of P-wave speed in km/s at different depths are shown. Only areas with an associated diagonal resolution greater than 0.2 are shown. Areas with smaller resolution are faded out. Vp is mapped at six depths below sea level z : a) z = 3 km, b) z = 15 km, c) z = 25 km, d) z = 40 km, e) z = 55 km, and f) z = 70 km.

Earthquake Locations with a 3D Velocity Model

We identified 1649 earthquakes between October 2001 and March 2003 by picking P and S arrival times. All these earthquakes were relocated using 3D velocity models (Figures 2 and 3) and the local magnitude was determined using the routine *dbml* from the BRTT Antelope Package. Earthquake local magnitudes range from 1 to 5.5.

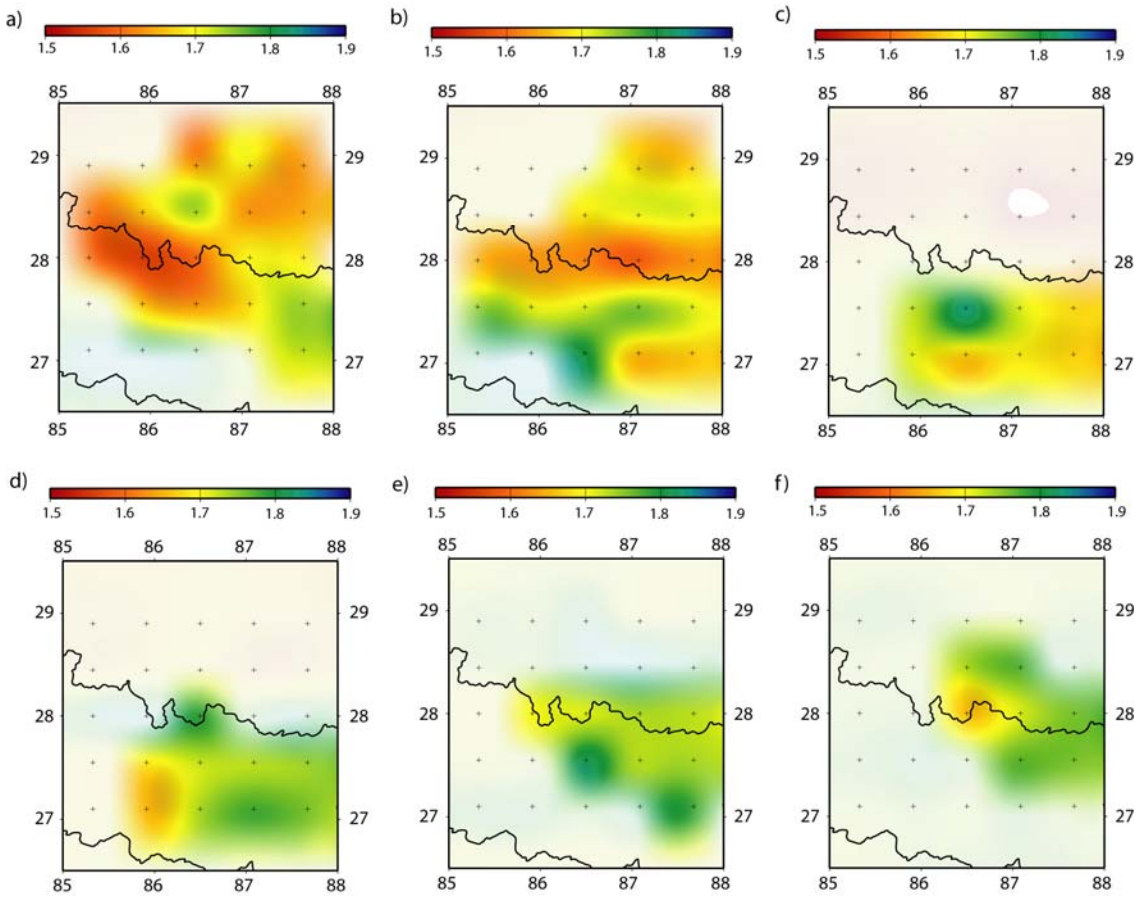

Figure 3. **Horizontal sections of P to S-wave speed ratios (Vp/Vs) at different depths are shown. Only areas with an associated diagonal resolution greater than 0.2 are shown. Areas with smaller resolution are faded out. Vp/Vs is mapped at six depths below sea level *z* : a) z = 3 km, b) z = 15 km, c) z = 25 km, d) z = 40 km, e) z = 55 km, and f) z = 70 km.**

Earthquake locations were encountered using the NonLinLoc software (Lomax, 2004), which determines probabilistic, non-linear earthquake locations in 3D structures. We use the model illustrated in Figures 2 and 3 in order to locate the set of 1649 earthquakes. NonLinLoc uses a global optimization method where for each set of arrival times corresponding to one earthquake, the whole model space is searched, preventing convergence towards local minima. This method gives better solutions than earthquake location algorithms used previously, which consisted of local optimization methods. We used a nested grid-search algorithm in order to find the location with the highest probability density function. The model was extended in all directions so that events out of the resolved portion of the velocity model could be located. Figure 4 shows a map view of the earthquake locations in the study area, with colors denoting hypocenter depth and sizes indicating earthquake local magnitude. Earthquake depths go from surface to approximately 90 km below sea level.

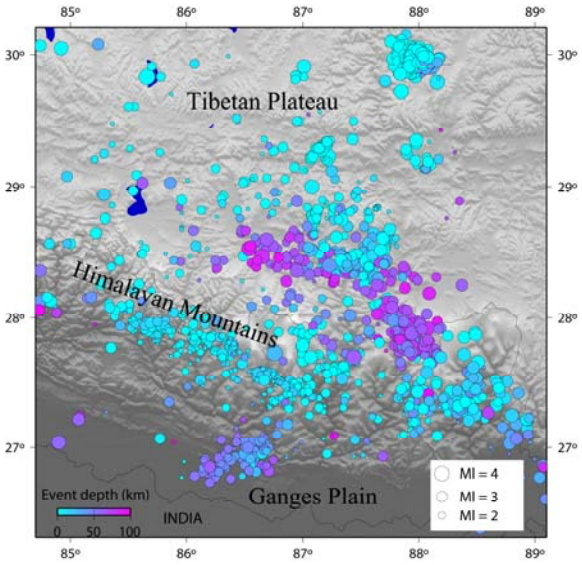

Figure 4. **Map view of the whole set of earthquake locations using the NonLinLoc software. Events are size-scaled by magnitude and color-scaled by depth.**

Moment Tensor and Source Parameter Analysis

We calculated moment tensor inversions for thirteen earthquakes using the moment tensor method of Ammon and Randall (1994) with data collected from the HIMNT experiment, the Bhutan PASSCAL network, and the Global Seismic Network (GSN, station LSA). We created Green's functions for the radial, transverse, and vertical components from 1D velocity models using the reflectivity method of Randall (1994). Since crustal thickness and topography vary dramatically across the study region, we used velocity models with variable speeds and Moho depths to obtain an average fault plane solution and focal depth. We modeled the whole waveform for each component of each station between 5–100 s. Figure 5 illustrates the lower hemisphere projections of the thirteen events at their epicenter locations. Focal mechanisms were verified with take-off angle and first motion polarities from the broadband data and with seismograms collected from the permanent short period vertical component network of the National Seismic Center of the Department of Mines and Geology of Nepal. Figure 6 illustrates the seismicity and focal mechanisms for earthquakes at focal depth range 60–100 km from the HIMNT experiment and four focal mechanism solutions from past studies. This cluster of earthquakes trending NW-SE and the mostly strike slip focal mechanisms suggest a possible shear zone under the Himalayas and the southern Tibetan Plateau.

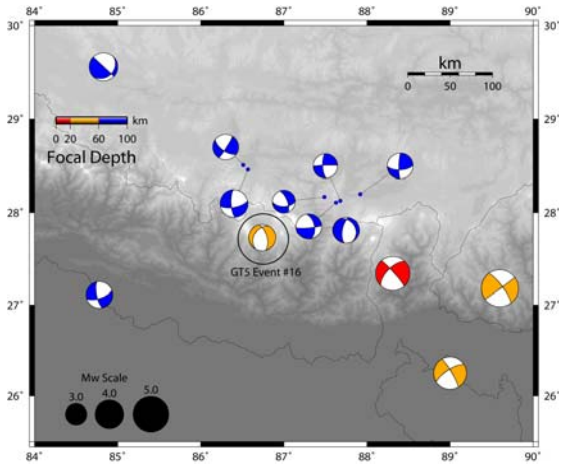

Figure 5. Focal mechanisms for thirteen events located in Figure 4. One earthquake (circled) was determined to be also a GT5 event.

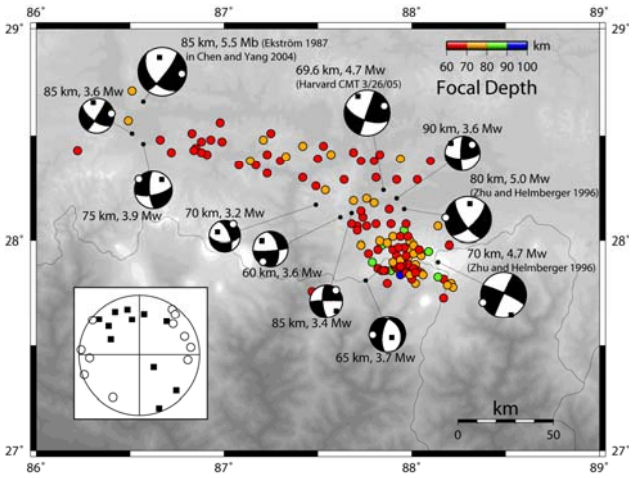

Figure 6. Fault plane solutions from this experiment coupled with solutions from other studies show predominant strike-slip faulting and possibly one normal faulting event 60–100 km under the Himalayas and the southern Tibetan Plateau. Insert illustrates lower hemisphere projections of P-axis orientations (closed squares) and T-axis orientations (open circles).

Ground Truth Events

After the use of advanced earthquake location algorithms we found hypocenters for hundreds of events detected as part of the HIMNT experiment. A subset of these events can be used to improve the database of seismic event ground thruth (GT) information for central and south Asia. According to Bondar et al. (2003), candidate events at the GT5 confidence level must be recorded at 10 or more stations within 250 km, the azimuthal gap should be less than 110°, the secondary azimuthal gap has to be less than 160°, and at least one of the stations should locate within 30 km from the epicenter. A total of 33 of the earthquake events recorded by the HIMNT network meet the Bondar et al. (2003) criteria (Table 1, Figure 7). Their local magnitudes range from 1.61 to 3.79. Figure 7a illustrates the 95% confidence level ellipses for these events in map view. The hypocenter projections onto a north-south vertical plane with the 95% confidence level vertical error bars are shown in Figure 7b.

We determined the source parameters by moment tensor inversion for one GT5 event (#16 in Table 1, Figure 8). The other events were not analyzed for source parameters since their signal-to-noise ratios were not large enough for the moment tensor inversion method we used. A 1D velocity model was extracted from 3D tomographic velocity model for input into the moment tensor inversion. The hypocenter using the NonLinLoc software was at a depth of 26.25 ± 1.3 km while the minimum moment tensor depth was at 32 km. We did not correct for station elevations (2.2 km above sea level on average for this event) for the moment tensor inversion, so the focal depth should be corrected to at least ~ 29.8 km.

Table 1. Candidate events at the GT5 confidence level

	ºN	ºE	Depth (km)	Date	Time (UTC)	M_L
1	27.5579	86.7601	14.75	10/27/2001	16:48:49	2.46
2	26.9256	86.5315	42.00	12/20/2001	7:36:34	2.41
3	27.0336	86.6301	32.00	1/7/2002	18:05:26	2.03
4	28.3926	86.7775	67.75	1/13/2002	14:32:09	2.88
5	27.3554	86.747	2.25	1/21/2002	3:47:20	2.41
6	27.5669	86.6307	13.00	1/25/2002	20:32:55	1.9
7	27.5646	86.6282	11.00	1/25/2002	21:48:21	2.5
8	27.7851	86.3894	25.50	2/3/2002	7:41:58	3.79
9	27.7986	86.3817	9.00	2/3/2002	10:04:12	2.32
10	26.7569	86.3803	54.25	3/1/2002	23:21:06	2.53
11	27.5196	86.8894	17.00	3/17/2002	22:05:11	2.6
12	27.5916	86.6333	14.50	3/26/2002	18:48:48	2.27
13	27.5174	86.1233	15.25	4/9/2002	7:23:23	2.98
14	27.8009	86.191	6.00	4/25/2002	6:22:01	2.14
15	26.7681	86.2518	48.50	4/30/2002	18:33:02	2.47
16	27.7289	86.7555	26.25	5/2/2002	17:35:30	4.2
17	27.8526	86.2799	18.00	6/22/2002	22:25:13	2.7
18	27.1754	86.8022	43.25	7/2/2002	20:28:52	2.27
19	27.2834	87.1848	< 1	7/12/2002	17:25:03	1.61
20	27.0741	85.771	5.25	7/23/2002	23:16:47	2.96
21	28.7459	87.3071	6.00	7/24/2002	8:33:20	2.45
22	28.6829	87.7452	5.00	8/1/2002	20:29:30	3.33
23	28.6671	86.5064	77.25	8/7/2002	17:29:40	2.62
24	27.6456	86.4759	7.25	8/16/2002	6:23:47	2.97
25	28.5546	87.7232	12.25	9/2/2002	12:02:52	2.53
26	27.3644	87.3627	24.00	9/3/2002	8:46:39	2.08
27	27.7199	85.9218	< 1	9/6/2002	14:46:04	1.93
28	28.5794	86.86	64.25	9/22/2002	9:34:59	2.33
29	27.5804	86.6104	19.25	10/2/2002	21:35:14	2.81
30	28.9259	86.3188	< 1	10/16/2002	21:05:35	2.58
31	28.9146	86.3034	< 1	10/16/2002	21:08:09	2.39
32	27.0561	87.4512	16.00	10/25/2002	14:58:27	2.62
33	28.5546	86.9982	59.50	8/26/2002	2:31:53	2.6

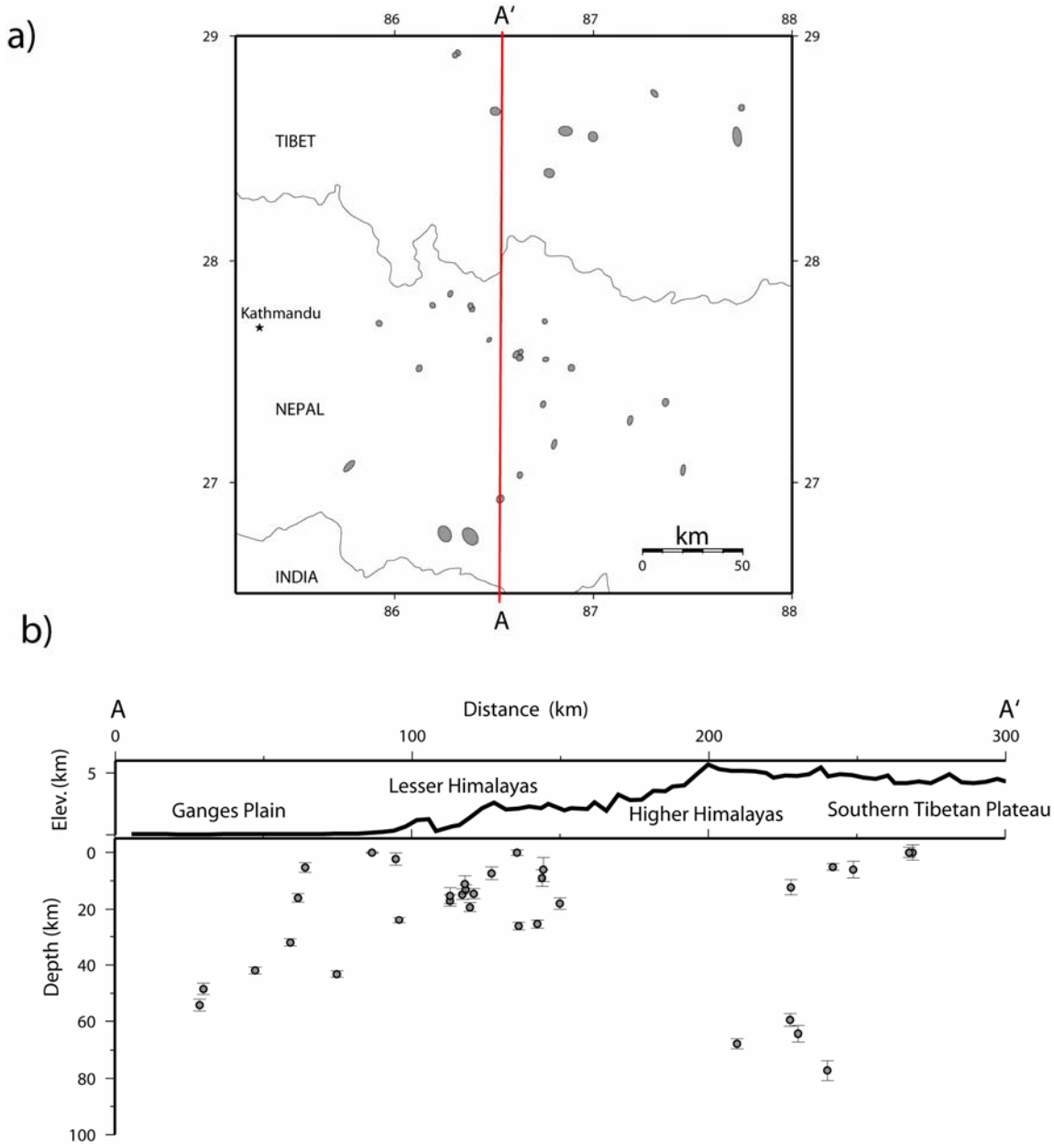

Figure 7. Location of the candidates for GT5 events (Bondar et al., 2003). a) Map view of the candidate event locations with their associated 95% confidence level ellipses. Red line marks the location of cross-section in part (b). b) North-south cross-section of the study area with the event projections and their associated 95% confidence level vertical uncertainties.

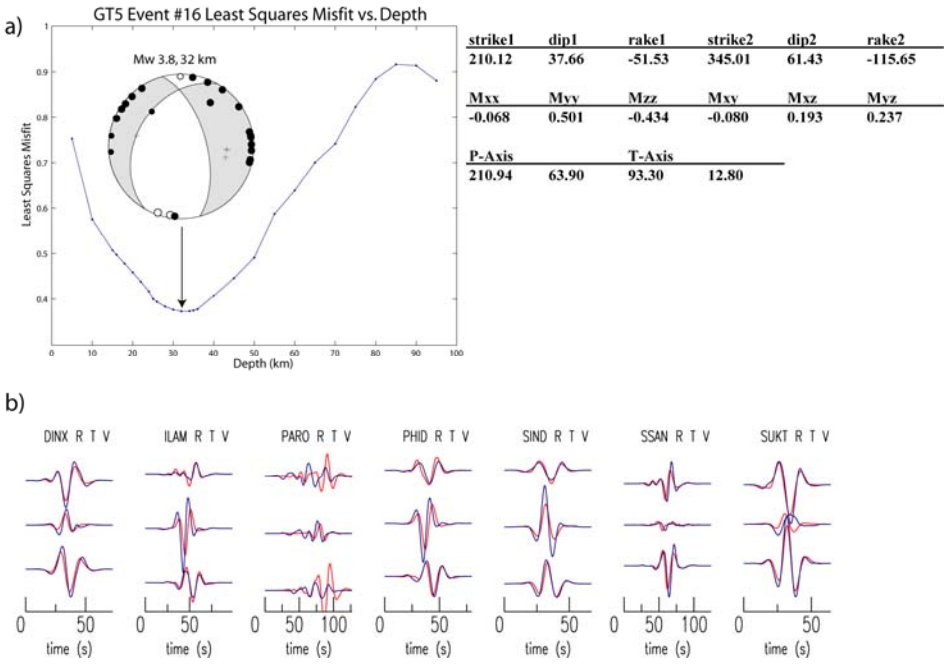

Figure 8. Moment tensor solution for GT event #16 (Table 1) using the 1D velocity extracted from the 3D tomographic velocity model in this analysis. a) A minimum misfit normal faulting solution occurs at a focal depth of 32 km or 29.8 km relative to sea level. Compressive first motion (closed circles), dilational first motion (open circles). b) Data (blue) plotted versus synthetic (red) seismograms at the 32 km focal depth solution.

CONCLUSIONS AND RECOMMENDATIONS

Use of in-country networks contributes to ground truth location determination in central Asia, important for validation of regional velocity models and correction surfaces. Through travel time and moment tensor inversions, we have obtained a regional 3D velocity model profile and source parameters for thirteen events. Examination of the 1649 earthquakes detected by the HIMNT network indicated 33 high-quality ground truth events not included in global catalogs. These ground truth events will contribute to the National Nuclear Security Administration (NNSA) Knowledge Base, which will be used to calibrate station-centric correction surfaces and increase the ability to accurately locate and identify seismic events in these regions.

REFERENCES

Ammon, C. J., G. E. Randall (1994). Deviatoric moment tensor inversion, http//:eqseis.geosc.psu.edu/~cammon/HTML/MTinvDocs/mtinv01.html, 2005.

Bondar, I., S. C. Myers, E.R. Engdahl, and E.A. Bergman (2004). Epicentre accuracy based on seismic network criteria, *Geophys. J. Int.* 156: 483–496.

Chen, W. P. and Z. H. Yang (2004). Earthquakes beneath the Himalayas and Tibet: Evidence for strong lithospheric mantle, *Science* 304: 1949–1952.

Eberhart-Phillips, D. (1986). Three-dimensional velocity structure in the northern California coast ranges from inversion of local earthquake arrival times, *Bull. Seismol. Soc. Am.* 76: 1025–1052.

Eberhart-Phillips, D. (1990. Three-dimensional P and S velocity structure in the Coalinga region, California, *J. Geophys. Res.* 95: 15343–15363.

Eberhart-Phillips, D. and A. J. Michael (1998). Seismotectonics of the Loma Prieta, California, region determined from three-dimensional Vp, Vp/Vs and seismicity, *J. Geophys. Res.* 103: 21099–21120.

Harvard University Department of Geological Sciences (2005), *Centroid Moment Tensor Catalog*, www.seismology.harvard.edu/CMTsearch.html

Husen, S., E. Kissling, and E. Flueh (2000). Local earthquake tomography of shallow subduction in north Chile: A combined on-shore and off-shore study, *J. Geophys. Res.* 105: 28183–28198.

Lomax, A. (2004). Probabilistic, non-linear, global-search earthquake location in 3D media, NonLinLoc Version 3.03, Anthony Lomax Scientific Software, Mouans-Sartoux, France.

Menke, W. (1989). *Geophysical Data \Analysis: Discrete Inverse Theory.* Academic Press.

Michelini, A. and T. V. McEvilly (1991). Seismological studies at Parkfield.—I. Simultaneous inversion for velocity structure and hypocenters using cubic B-splines parameterization, *Bull. Seismol. Soc. Am.* 81: 524–552.

Randall, G. E. (1994). Efficient calculation of complete differential seismograms for laterally homogenous earth models, *Geophys. J. Int.* 118: 245–254.

Thurber, C. (1983). Earthquake locations and three-dimensional crustal structure in the Coyote Lake area, central California, *J. Geophys. Res*. 88: 8226–8236.

Thurber, C. (1993). Local earthquake tomography: Velocities and Vp/Vs—Theory, in *Seismic Tomography: Theory and Practice*, H. M. Iyer and K. Hirahara (Eds.). New York: Chapman and Hall, pp. 563–583.

Toomey, D. R., and G. R. Foulger (1989). Tomographic inversion of local earthquake data from the Hengill-Grensdalur central volcano complex, Iceland, *J. Geophys. Res.* 94: 17497–17510.

Zhu, L. P. and D. V. Helmberger (1996). Intermediate depth earthquakes beneath the India-Tibet collision zone, *Geophys. Res. Lett*. 23: 435–438.